Materials Science and Applications, 2018, *, *-*
http://www.scirp.org/journal/msa
ISSN Online: 2153-1188
ISSN Print: 2153-117X

Patterned nanofoam fabrication from a variety of materials via femtosecond laser pulses

James A. Grant-Jacob*, Benita S. Mackay, James A. G. Baker, Yunhui Xie, Michael D. T. McDonnell, Daniel J. Health, Matthew Praeger, Robert W. Eason and Ben Mills

Optoelectronics Research Centre, University of Southampton, Southampton, UK
Email: *jagj1v11@soton.ac.uk

How to cite this paper: Author 1, Author 2 and Author 3 (2018) Paper Title. ******, *, *-*.
http://dx.doi.org/10.4236/***.2018.*****

Received: **** **, ***
Accepted: **** **, ***
Published: **** **, ***

Copyright © 2018 by author(s) and Scientific Research Publishing Inc.
This work is licensed under the Creative Commons Attribution International License (CC BY 4.0).
http://creativecommons.org/licenses/by/4.0/
Open Access

Abstract

High-repetition-rate femtosecond lasers enable the precise production of nanofoam from a wide range of materials. Here, the laser-based fabrication of nanofoam from silicon, borosilicate glass, soda-lime glass, gallium lanthanum sulphide and lithium niobate is demonstrated, where the pore size of the nanofoam is shown to depend strongly on the material used. In addition, the patterning of nanofoam on a glass slide, with fabricated pattern pixel resolution of ~ 35 μm, is demonstrated.

Keywords

Laser Ablation, Nanofibres, Nanofoam, QR code, Patterning, Lithium Niobate, Gallium Lanthanum Sulphide, Silicon, Silica

1. Introduction

A class of porous nanostructured materials, known as nanofoams [1–3], can be made via a variety of methods, such as laser ablation [4–6]. Laser-based nanofoam fabrication offers the potential for control over the precise location at which the nanofoam is generated. Such fabrication generally involves using a laser operating at a high repetition rate (usually at least 250 kHz) delivering femtosecond pulses onto the surface of a material [7]. Upon incidence on the material, the laser pulses can undergo nonlinear absorption, leading to the generation of a plasma via multiphoton ionization and subsequent avalanche ionization [4,8–10]. The high number of ultra-short pulses incident on one area of the material, in a

short enough time, can lead to the build-up of thermal energy causing the surrounding material to melt [11–16]. During this process, molten droplets and jets of materials are ejected [4,14], which, due to their small size, cool rapidly and solidify to form nanofibres that can intertwine to form nanofoam [17]. The volume of the nanofoam, the pore size, and nanofibre width, can depend on fabrication parameters such as the speed of translation of the sample beneath the incident laser beam and the focal conditions of the laser [18].

Such fibrous nanostructures have received great interest recently, owing to their optical and mechanical properties. Potential applications include subwavelength-diameter glass wires for microscale photonic devices [19] and evanescent nanosensors [20], nanoscale fibres for advancing silicon photonics [21], and polymer nanofibres for biomedical applications such as tissue templates [22].

Here, we use ~ 150 fs duration laser pulses to fabricate nanofoam from silicon (a common material used in electronics and mid-IR photonics) [6,23], silica-based glass (used in a wide range of photonics applications) [24], gallium lanthanum sulphide, also known as GLS (a material used in active and passive infrared applications) [25], and lithium niobate (a ferroelectric material used in nonlinear optical applications) [26,27]. We also demonstrate the ability to fabricate patterned regions of nanofoam on a borosilicate glass slide.

2. Experimental Setup

The laser-based fabrication of nanofoam generally requires the raster-scanning of a focussed laser spot across the material surface. The laser pulse energy, laser focus spot size, the spacing between adjacent raster-scanned lines and the raster-scan line speed are all parameters that can be optimized for the fabrication process. **Figure 1** shows a schematic of the experimental setup used for nanofoam fabrication. Ultrashort pulses of ~ 150 fs duration and central wavelength of 800 nm, from an ultrafast Ti:sapphire laser system operating at a repetition rate of 250 kHz, delivering an energy of ~ 4 μJ per pulse, were used to fabricate the nanofoam. The laser pulses passed through a computer-controlled shutter and a 4 mm diameter circular aperture, to convert a Gaussian spatial intensity into one that closely resembled a top-hat spatial intensity. Subsequently, the pulses were demagnified using a 50x microscope objective lens (Nikon LU Plan, NA = 0.55) and imaged to a beam diameter of ~ 4 μm on the surface of a material, which resulted in a laser pulse energy density of ~ 15 J cm^{-2} at the surface of the material. The materials were mounted on a 3-axis stage that was computer controlled to allow automated raster-scan translation of the material, hence effectively scanning the laser focus along the surface of the material. This enabled the fabrication of individual lines of nanofoam to form a contiguous region of nanofoam, as described in previous work [18].

For consistency, we used a raster-scan line speed of 1 mms^{-1} and raster-scan line separation of 5 μm for all materials, where the lateral dimensions of the fabricated nanofoam was on the order of a few hundred microns. Five different materials, namely silicon, borosilicate

glass, sodalime glass, GLS and lithium niobate were investigated.

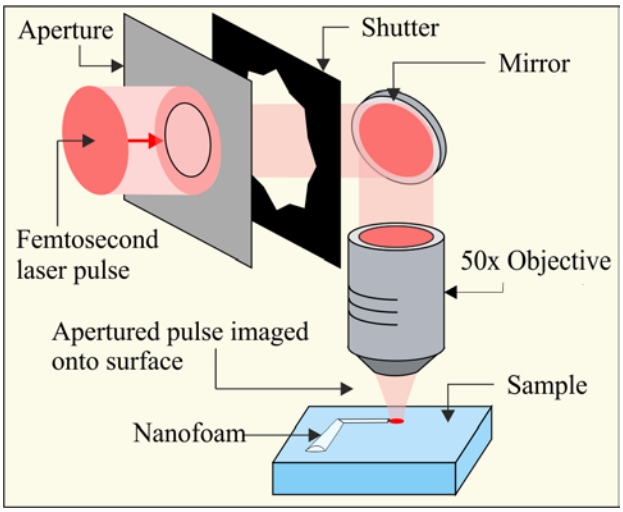

Figure 1. Schematic of the experimental setup for fabrication of nanofoam on the surface of a material.

3. Results and Discussion

In this experimental section, results from each of the five materials are presented in Sections 3.1 to 3.5. In each case, a low-resolution and high-resolution scanning electron microscope (SEM) image is presented, along with analysis of the nanofoam parameters. Here, the pore size and the nanofibre width were calculated directly from the high-resolution images by using image analysis software to measure the mean width over 10 positions. A comparison is presented in Section 3.6, and results for high-precision patterning are shown in Section 3.7. Laser and raster-scan parameters were constant for all materials, and hence a direct comparison can be made.

3.1 Silicon

The nanofoam fabricated from the polished surface of a p-type (100) silicon wafer is highlighted in the SEM image shown in **Figure 2(a)**. Fragments of coalesced material and nanofibers are visible up to a few hundred microns away from the nanofoam block, demonstrating how far the ablated material can be ejected. Although from the image in Figure 2(a), the nanofoam block appears to be an amalgamation of material, as seen from a higher magnification image of the nanofoam (**Figure 2(b)**), the width of the fibres that make up the nanofoam are ~ 90 nm wide and the average pore size is ~ 1.1 micron in width.

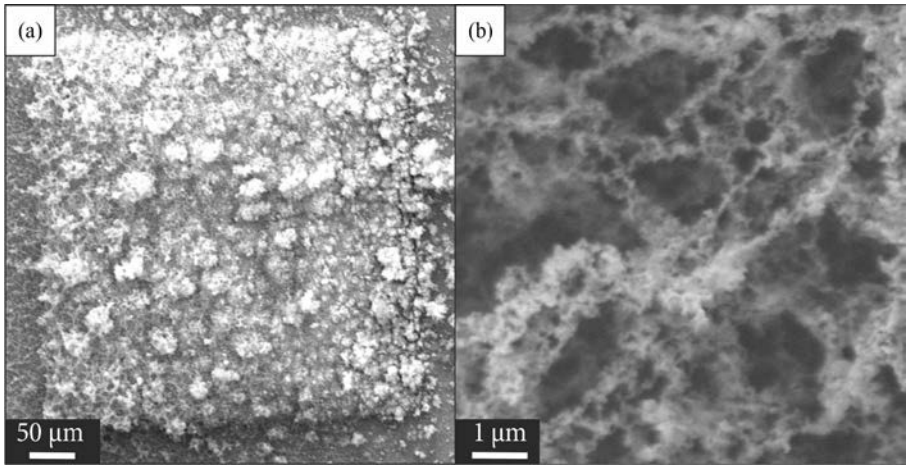

Figure 2. SEM images of the silicon nanofoam showing a) the 0.45 mm by 0.45 mm total area and b) higher magnification detail of the nanofoam fibres.

3.2 Borosilicate Glass

Under the same conditions as the fabrication of silicon, a square region of borosilicate nanofoam was fabricated from a borosilicate glass slide (BK7, 75x25x0.7mm). An SEM image of the nanofoam region is presented in **Figure 3(a)**. In this case there is less visible ejection of material outside of the ablated region, and, in particular, far fewer filamentary structures are present. The ejected material instead takes the form of very small particles with occasional larger clumps. Determined from the higher magnification image in **Figure 3(b)**, an average nanofibre width of ~ 120 nm was calculated, and an average pore width of ~ 1.2 microns was calculated.

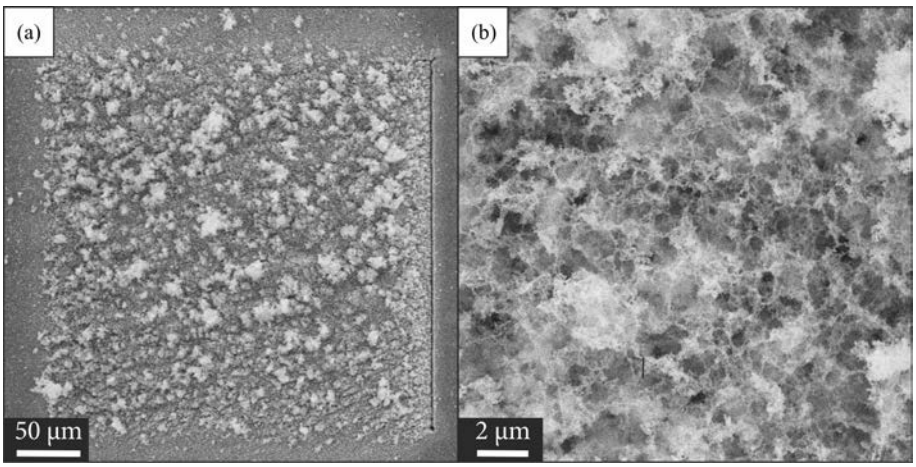

Figure 3. SEM images of the borosilicate nanofoam showing a) the 0.3 mm by 0.3 mm total area and b) higher magnification detail of the nanofoam fibres.

3.3 Soda Lime Glass

To provide a comparison for a different type of silica glass, nanofoam was fabricated from soda lime glass, which in this work was in the form of a coverslip (24x50x0.16mm). The nanofoam produced was visually different from those produced from the borosilicate glass. From **Figure 4(a)**, the average pore size of ~ 2.3 μm and nanofiber width of ~ 300 nm is shown.

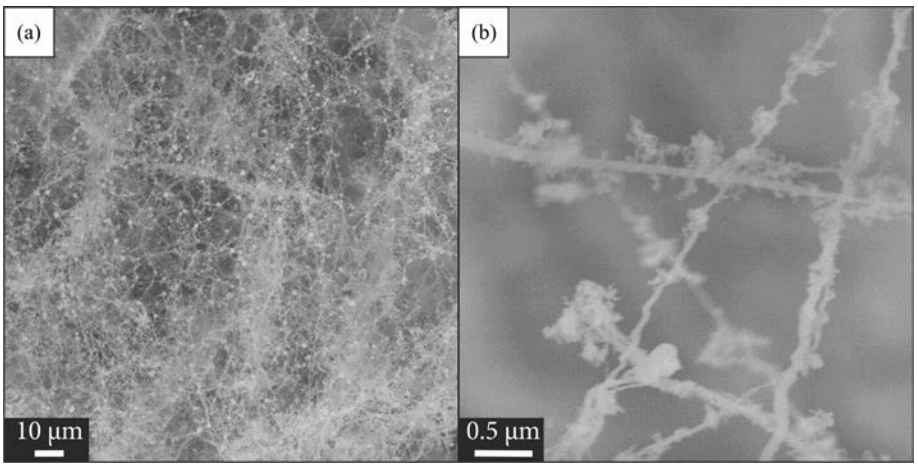

Figure 4. SEM images of the soda-lime nanofoam showing a) the presence of beads of material at the end of the nanofibers, and b) higher magnification detail for single nanofibers.

3.4 Gallium Lanthanum Sulphide

From the SEM image shown in **Figure 5(a)**, it is evident that the nanofoam structure produced average pore size of ~ 2.3 μm and nanofiber width of ~ 300 nm. Using a scalpel to dig into the nanofoam volume and drag the nanofoam, it was also possible to stretch the nanofoam, which then remained in its deformed position as shown in **Figure 5(b)**.

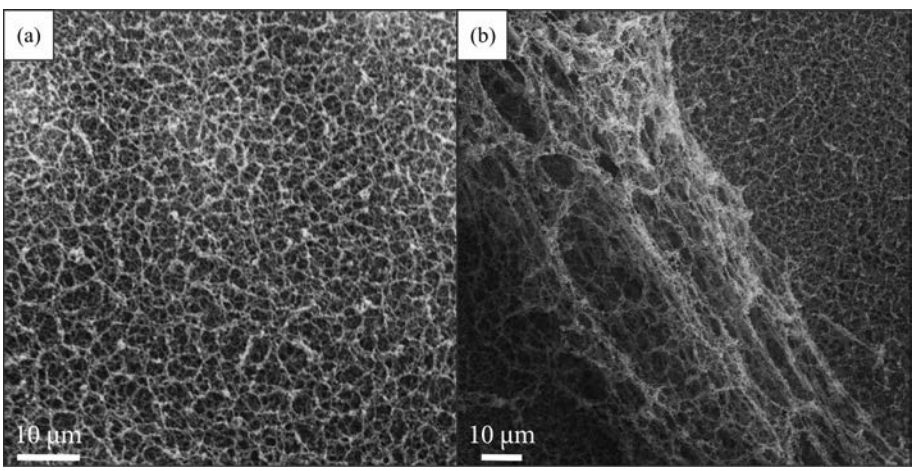

Figure 5. High resolution SEM images of the GLS nanofoam showing a) nanofoam detail

and b) the ability to mechanically deform the nanofoam.

3.5 Lithium Niobate

Compared to the other materials the nanofoam produced via the ablation of lithium niobate was produced away from the ablation area, and not in the location of laser irradiation, as shown in **Figure 6(a)**. The nanofoam appears to have been generated up to ~ 1 mm away from the laser irradiated region. There also appears to be a directionality to the nanofibres of the foam. The average nanofibre width was ~ 750 nm and the average pore width was ~ 7 µm.

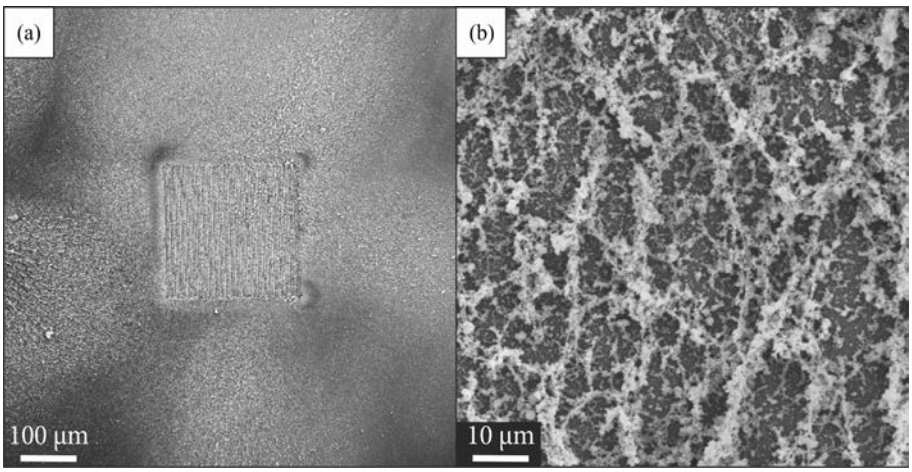

Figure 6. SEM images of the lithium niobate nanofoam showing a) the 0.25 mm by 0.25 mm total area and b) higher magnification detail of the nanofoam fibres, outside the laser irradiated region, where in general the nanofibers are orientated in the preferential direction.

3.6 Comparison for the Materials

Table 1 shows a comparison between the nanofoam materials fabricated, for the average pore width and the average nanofiber width, as measured from the SEM images in Sections 3.1 to 3.5. The results indicate a correlation between average pore width and nanofibre width.

Table 1. Table displaying the approximate avarage pore width and approximate nanofibre width of the nanofoams produced from the different materials.

Material	Average pore width (µm)	Average nanofibre width (nm)
Silicon	1.1	90
Borosilicate Glass	1.2	120
Soda Lime Glass	4.88	340
GLS	2.3	300
Lithium Niobate	7	750

This correlation can be seen clearly from the plot in **Figure 7(a)**, which shows average pore width versus average nanofibre width. Plotted in **Figure 7(b)** are the average pore width and average nanofibre width as a function of bulk material density. In this plot the trend shows that increasing density increases average pore width and nanofibre width. A similar increasing trend in average pore width and nanofibre width is also observed with increasing thermal expansion coefficient, as shown **Figure 7(c)**. These trends are perhaps understandable owing to less dense material being more easily ablated with material having more energy and travelling further from the material, thus creating larger pores. Likewise, ejected melted material that expands faster due to a higher thermal expansion would likely lead to larger pores.

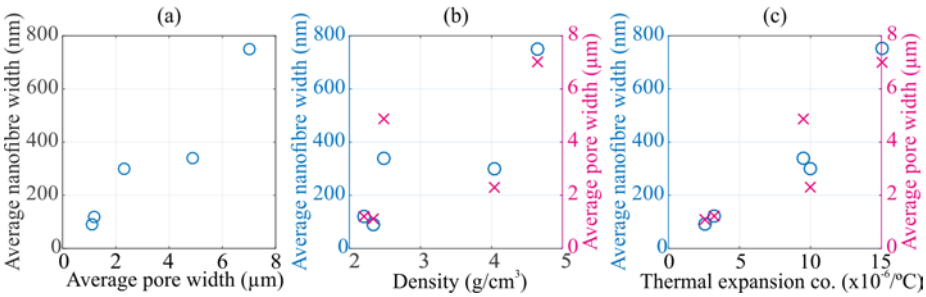

Figure 7. (a) Average pore width as a function of nanofibre width from the nanofoams produced in this work. Average pore width and average nanofibre width as a function of (b) density of the bulk material and (c) thermal expansion coefficient of the material. Values of density and thermal expansion coefficient at 25 °C obtained from [28–31].

3.7 Nanofoam patterning

In order to demonstrate the versatility of the fabrication method and potential applications, we chose to produce patterned areas of nanofoam. For this demonstration, the computer-controlled shutter was automatically opened and closed, whilst the laser focus was continually raster-scanned over the surface of the material, in order to laser irradiate the intended pattern. The size of the patterns was chosen as a balance between minimum time of fabrication and maximum possible resolution for potential imaging using a smartphone camera, for example. The patterns chosen for the nanofoam fabrication were a wheel and a QR code, where the designs were implemented by the automated stages via Matlab and LabVIEW. Both patterns were fabricated on a borosilicate glass slide, each over 2 mm x 2 mm square area. For proof of principle and ease of machining in straight lines, the patterns were chosen to be formed of square pixels. Each pixel on the 32 pixel x 32 pixel wheel image corresponded to a 65 μm x 65 μm machined area, and each pixel on the 16 pixel x 16 pixel QR code corresponded to a patterned pixel of 35 μm x 35 μm machined area.

An SEM image of the wheel pattern is shown in **Figure 8(a)**, where the white parts of the image correspond to the regions of nanofoam. The smearing in the image is due to air currents blowing some debris particles during fabrication of the nanofoam. An optical microscope image of the nanofoam QR code is shown in **Figure 8(b)**, where regions of

nanofoam appear as grey, and the non-ablated glass as white. Inset to both figures is the monochrome bitmap pattern loaded into the Matlab and LabVIEW program.

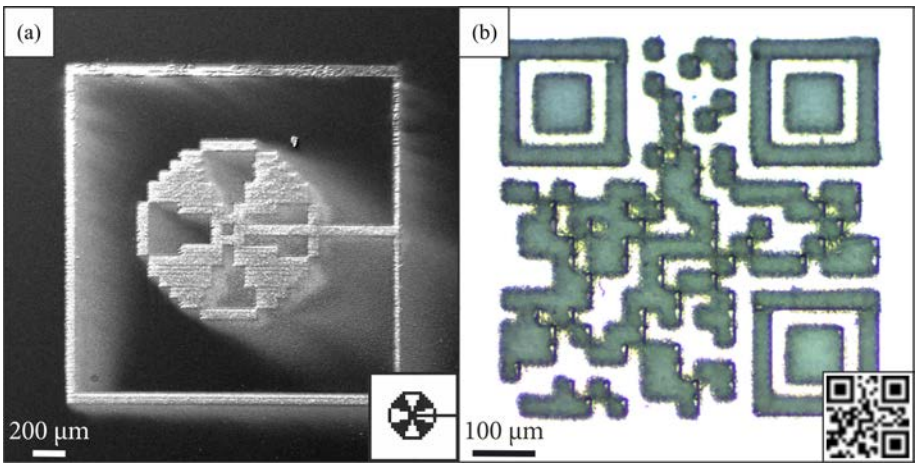

Figure 8. Demonstration of patterned nanofoam, showing a) an SEM image of a wheel pattern and (b) a microscope image of a QR code.

4. Conclusions

In conclusion, we have demonstrated that femtosecond ablation can be used to fabricate nanofoam from a range of materials, where the porosity and volume of the nanofoam and the width of the wires were shown to be dependent on the particular material. More specifically, the pore width and nanofibre width appeared to increase with density and thermal expansion coefficient of the material. We also demonstrated the fabrication of patterned nanofoam, including a QR code of glass nanofoam. Further work will focus on the optimisation of the size and structure of the nanofoam via machine learning [32].

Acknowledgements

The authors are grateful to the Engineering and Physical Sciences Research Council (EPRSC) under grant no. EP/N03368X/1. The RDM data for this paper can be found at https://doi.org/10.5258/SOTON/D0753

References

[1] Bag S., Trikalitis P.N., Chupas P.J., Armatas G.S., and Kanatzidis M.G. (2007) Porous semiconducting gels and aerogels from chalcogenide clusters. *Science*, **317**, 490–3. http://dx.doi.org/10.1126/science.1142535

[2] Sun H., Xu Z., and Gao C. (2013) Multifunctional, Ultra-Flyweight, Synergistically Assembled Carbon Aerogels. *Adv. Mater.*, **25**, 2554–60. http://dx.doi.org/10.1002/adma.201204576

[3] Brock S.L. (2007) Materials science. Filling a void. *Science*, **317**, 460–1. http://dx.doi.org/10.1126/science.1146517

[4] Venkatakrishnan K., Vipparty D., and Tan B. (2011) Nanofibre fabrication by femtosecond laser ablation of silica glass. *Opt. Express*, **19**, 15770–6. http://dx.doi.org/10.1364/OE.19.015770

[5] Juodkazis S., Misawa H., Louchev O.A., and Kitamura K. (2006) Femtosecond laser ablation of chalcogenide glass: explosive formation of nano-fibres against thermo-capillary growth of

micro-spheres. *Nanotechnology*, **17**, 4802–5. http://dx.doi.org/10.1088/0957-4484/17/19/003

[6] Zhang Y.F., Tang Y.H., Wang N., Yu D.P., Lee C.S., Bello I., and Lee S.T. (1998) Silicon nanowires prepared by laser ablation at high temperature. *Appl. Phys. Lett.*, **72**, 1835. http://dx.doi.org/10.1063/1.121199

[7] Rode A.V., Gamaly E.G., and Luther-Davies B. (2000) Formation of cluster-assembled carbon nano-foam by high-repetition-rate laser ablation. *Appl. Phys. A Mater. Sci. Process.*, **70**, 135–44. http://dx.doi.org/10.1007/s003390050025

[8] Feit M.D., Komashko A.M., and Rubenchik A.M. (2004) Ultra-short pulse laser interaction with transparent dielectrics. *Appl. Phys. A*, **79**, 1657–61. http://dx.doi.org/10.1007/s00339-004-2683-1

[9] Kaiser A., Rethfeld B., Vicanek M., and Simon G. (2000) Microscopic processes in dielectrics under irradiation by subpicosecond laser pulses. *Phys. Rev. B*, **61**, 11437–50. http://dx.doi.org/10.1103/PhysRevB.61.11437

[10] Brodeur A., and Chin S. (1998) Band-Gap Dependence of the Ultrafast White-Light Continuum. *Phys. Rev. Lett.*, **80**, 4406–9. http://dx.doi.org/10.1103/PhysRevLett.80.4406

[11] Kasaai M.R., Kacham V., Theberge F., and Chin S.L. (2003) The interaction of femtosecond and nanosecond laser pulses with the surface of glass. *J. Non. Cryst. Solids*, **319**, 129–35. http://dx.doi.org/10.1016/S0022-3093(02)01909-9

[12] Tamaki T., Watanabe W., and Itoh K. (2006) Laser micro-welding of transparent materials by a localized heat accumulation effect using a femtosecond fiber laser at 1558 nm. *Opt. Express*, **14**, 10460–8. http://dx.doi.org/10.1364/OE.14.010460

[13] Koubassov V., Laprise F.J., Théberge F., Förster E., Sauerbrey R., Müller B., Glatzel U., and Chin S.L. (2004) Ultrafast laser-induced melting of glass. *Appl. Phys. A Mater. Sci. Process.*, **79**, 499–505. http://dx.doi.org/10.1007/s00339-003-2474-0

[14] Tokarev V.N., Lazare S., Belin C., and Debarre D. (2004) Viscous flow and ablation pressure phenomena in nanosecond UV laser irradiation of polymers. *Appl. Phys. A*, **79**, 717–20. http://dx.doi.org/10.1007/s00339-004-2693-z

[15] Korte F., Koch J., and Chichkov B.N. (2004) Formation of microbumps and nanojets on gold targets by femtosecond laser pulses. *Appl. Phys. A*, **79**, 879–81. http://dx.doi.org/10.1007/s00339-004-2590-5

[16] Ben-Yakar A., Byer R.L., Harkin A., Ashmore J., Stone H. a., Shen M., and Mazur E. (2003) Morphology of femtosecond-laser-ablated borosilicate glass surfaces. *Appl. Phys. Lett.*, **83**, 3030. http://dx.doi.org/10.1063/1.1619560

[17] Courtier A.F., Grant-Jacob J.A., Ismaeel R., Heath D.J., Brambilla G., Stewart W.J., Eason R.W., and Mills B. (2017) Laser-based fabrication of nanofoam inside a hollow capillary. *Mater. Sci. Appl.*, 8(12), 829-837. http://dx.doi.org/10.4236/msa.2017.812060

[18] Grant-Jacob J.A., Mills B., and Eason R.W. (2014) Parametric study of the rapid fabrication of glass nanofoam via femtosecond laser irradiation. *J. Phys. D. Appl. Phys.*, **47**, 55105. http://dx.doi.org/10.1088/0022-3727/47/5/055105

[19] Tong L., Gattass R.R., Ashcom J.B., He S., Lou J., Shen M., Maxwell I., and Mazur E. (2003) Subwavelength-diameter silica wires for low-loss optical wave guiding. *Nature*, **426**, 816.

[20] Brambilla G. (2010) Optical fibre nanowires and microwires: a review. *J. Opt.*, **12**, 43001.

[21] Liu Z.Q., Zhou W.Y., Sun L.F., Tang D.S., Zou X.P., Li Y.B., Wang C.Y., Wang G., and Xie S.S. (2001) Growth of amorphous silicon nanowires. *Chem. Phys. Lett.*, **341**, 523–8.

[22] Huang Z.-M., Zhang Y.-Z., Kotaki M., and Ramakrishna S. (2003) A review on polymer nanofibers by electrospinning and their applications in nanocomposites. *Compos. Sci. Technol.*, **63**, 2223–53.

[23] Reed G.T., Mashanovich G., Gardes F.Y., and Thomson D.J. (2010) Silicon optical modulators. *Nat. Photonics*, **4**, 518. http://dx.doi.org/10.1038/nphoton.2010.179

[24] Ikushima A.J., Fujiwara T., and Saito K. (2000) Silica glass: A material for photonics. *J. Appl. Phys.*, **88**, 1201–13. http://dx.doi.org/10.1063/1.373805

[25] Schweizer T., Brady D.J., and Hewak D.W. (1997) Fabrication and spectroscopy of erbium doped gallium lanthanum sulphide glass fibres for mid-infrared laser applications. *Opt.*

Express, **1**, 102–7. http://dx.doi.org/10.1364/OE.1.000102

[26] Abernethy J.A., Gawith C.B.E., Eason R.W., and Smith P.G.R. (2002) Demonstration and optical characteristics of electro-optic Bragg modulators in periodically poled lithium niobate in the near-infrared. *Appl. Phys. Lett.*, **81**, 2514–6. http://dx.doi.org/10.1063/1.1510964

[27] Weis R.S., and Gaylord T.K. (1985) Lithium niobate: summary of physical properties and crystal structure. *Appl. Phys. A*, **37**, 191–203. http://dx.doi.org/10.1007/BF00614817

[28] Cystran (2018) Silicon. https://www.crystran.co.uk/optical-materials/silicon-si.

[29] Cystran (2018) Gallium Lanthanum Sulphide. https://www.crystran.co.uk/optical-materials/gallium-lanthanum-sulphide-gls.

[30] Ashby M.F. (2013) Chapter 15 - Material profiles. *Materials and the Environment (Second Edition)* ed M F Ashby (Boston: Butterworth-Heinemann) pp 459–595 http://dx.doi.org/https://doi.org/10.1016/B978-0-12-385971-6.00015-4

[31] Gooch & Housego (2018) Lithium Niobate Wafers. https://goochandhousego.com/product-categories/ln-wafers/.

[32] Mills B., Heath D.J., Grant-Jacob J.A., and Eason R.W. (2018) Predictive capabilities for laser machining via a neural network. *Opt. Express*, **26**, 17245–53. http://dx.doi.org/10.1364/OE.26.017245